

The OGLE View of Microlensing towards the Magellanic Clouds. I. A Trickle of Events in the OGLE–II LMC data. ^{*}

L. Wyrzykowski^{1,2,†}, S. Kozłowski³, J. Skowron², V. Belokurov¹, M. C. Smith¹,
A. Udalski², M. K. Szymański², M. Kubiak², G. Pietrzyński^{2,4},

I. Soszyński², O. Szewczyk^{2,4} and K. Żebruń²

¹ *Institute of Astronomy, University of Cambridge, Madingley Road, Cambridge CB3 0HA, UK*

² *Warsaw University Astronomical Observatory, Al. Ujazdowskie 4, 00-478 Warszawa, Poland*

³ *Department of Astronomy, Ohio State University, 140 W. 18th Ave., Columbus, OH 43210, USA*

⁴ *Universidad de Concepción, Departamento de Física, Astronomy Group, Casilla 160-C, Concepción, Chile*

Accepted ... Received ...

ABSTRACT

We present the results from the OGLE–II survey (1996–2000) towards the Large Magellanic Cloud (LMC), which has the aim of detecting the microlensing phenomena caused by dark matter compact objects in the Galactic Halo (Machos).

We use high resolution HST images of the OGLE fields and derive the correction for the number of monitored stars in each field. This also yield blending distributions which we use in ‘catalogue level’ Monte Carlo simulations of the microlensing events in order to calculate the detection efficiency of the events.

We detect two candidates for microlensing events in the All Stars Sample, which translates into an optical depth of $0.43 \pm 0.33 \times 10^{-7}$. If both events were due to Macho the fraction of mass of compact dark matter objects in the Galactic halo would be 8 ± 6 per cent. This optical depth, however, along with the characteristics of the events, seems to be consistent with the self-lensing scenario, i.e., self-lensing alone is sufficient to explain the observed microlensing signal. Our results indicate a non-detection of Machos lensing towards the LMC with an upper limit on their abundance in the Galactic halo of 19 per cent for $M = 0.4M_{\odot}$ and 10 per cent for masses between 0.01 and $0.2 M_{\odot}$.

Key words: Cosmology: Dark Matter, Gravitational Lensing, Galaxy: Structure, Halo, Galaxies: Magellanic Clouds

1 INTRODUCTION

Although we are constantly learning new things about our Galaxy, some major questions about its structure still remain unanswered. Among them is the composition of the Galaxy halo. Solving this mystery has been the main goal of the large photometric surveys launched in the 1990s. The proposal of Paczyński (1986) has been realised by the surveys like MACHO (Alcock et al. 1993), OGLE (Udalski et al. 1993), EROS (Aubourg et al. 1993) and MOA (Yock 1998).

These groups continuously monitored millions of stars in both Magellanic Clouds in order to detect the transient amplification of brightness caused by objects crossing the observer–source line of sight in a phenomenon called gravitational microlensing (Paczynski 1996). The rate of such events depends on the number, mass and kinematics of objects populating the line of sight, in the disk and the halo of our Galaxy and in the Clouds. The main hypothesis all the surveys have been testing is whether the halo of our Galaxy contains dark matter in the form of the MAssive Compact Halo Objects, called Machos.

If the Galactic halo were entirely made of Machos, with masses between 10^{-8} and $10^8 M_{\odot}$, in a project like OGLE–II we should detect about five microlensing events per year towards the Large Magellanic Cloud (LMC), and the corresponding optical depth should be $\tau_{\text{Macho}} \approx 4.7 \times 10^{-7}$ (Ben-

^{*} Based on observations obtained with the 1.3 m Warsaw telescope at the Las Campanas Observatory of the Carnegie Institution of Washington.

† email: wyrzykow@ast.cam.ac.uk, name pronunciation: *Woo-cash Vizhikovskiy*

nett 2005). However, the actual optical depth measurements reported by the microlensing experiments are significantly smaller.

The MACHO collaboration presented a sample of 10 microlensing event candidates towards the LMC and concluded that the fraction of dark matter in Machos $f = M_{\text{Macho}}/M_{\text{halo}} \approx 20$ per cent, suggesting the existence of a new, previously unknown population of objects with masses $\sim 0.5M_{\odot}$ (Alcock et al. 2000b, Bennett 2005). Their estimate of the optical depth towards the LMC is $\tau_{\text{LMC}} = (1.0 \pm 0.3) \times 10^{-7}$. However, the EROS group reported a null result and derived an upper limit on the optical depth due to Machos of $\tau_{\text{Macho}} < 0.36 \times 10^{-7}$, which implies $f < 8$ per cent (Tisserand et al. 2007). MACHO’s sample of events is likely to have some contamination with variable stars, novae, and supernovae (Belokurov et al. 2003), and additional data indeed shows the presence of small contamination (Bennett et al. 2005). However, the optical depth we quote from MACHO has been corrected for this contamination (Bennett 2005). The large discrepancy between the results may be due to the different samples of stars used by these groups or the fact that they probe different regions of the LMC. However, it is unclear whether these fully explain the discrepancy.

Independent searches for Machos have also been carried out towards the Andromeda Galaxy (M31) using pixel-lensing method. For example, Calchi Novati et al. (2005) found 6 events and estimated the Machos halo mass fraction to be higher than 20 per cent. On the other hand, Belokurov et al. (2005) presented an automatic procedure that selects unambiguous microlensing events in a pixel light curve data set with a total of only 3 “gold-plated” candidates, thus emphasizing the lack of large numbers of clear-cut microlensing events towards the M31. de Jong et al. (2006) showed 14 events towards M31 and noticed that the observed event rate is consistent with the self-lensing predictions, however their results were still inconclusive, mainly due to low statistics.

In this paper we present the results of the search for microlensing events towards the Large Magellanic Cloud in the independent data set gathered by the Optical Gravitational Lensing Experiment (OGLE) in its second phase during the years from 1996 to 2000. The paper is organized as follows. First, the observational data are described along with the error bar correction procedure. Next, the event search algorithm and its results are presented. It is followed by the description of the analysis of blending and its impact on the optical depth measurement and the event’s detection efficiency. Finally, the optical depth is calculated and the results are discussed.

2 OBSERVATIONAL DATA

The data used in this paper were collected during the second phase of the OGLE survey, in the years 1996 – 2000 towards the Large Magellanic Cloud (LMC). The OGLE project used its own dedicated Warsaw Telescope in the Las Campanas Observatory, Chile. Details of the instrumentation for OGLE–II can be found in Udalski et al. (1997).

In brief, a 2k×2k CCD with a pixel size of 0.417 arcsec was operated in the drift-scan mode, giving an actual size for each observed field of 2k×8k. There were 21 fields observed towards the LMC covering a total of 4.72 square degrees.

Their locations are shown in Fig. 1. Fields are listed in Table 1, which contains the coordinates of centers of the fields, the number of good objects in the *I*–band, the blending-corrected number of stars (see Section 6) and the blending density group. By ‘good’, we mean all objects having at least 80 epochs during the entire time span of the OGLE–II (from about 15 to 25 per cent of all collected frames of a field) and mean magnitude brighter than 20.4 mag. The limiting magnitude was chosen to be at the peak of the observed luminosity function.

The images in the *I* and *V* bands were de-biased and flat-field corrected “on-the-fly”. The photometric pipeline was based on the Difference Image Analysis method (DIA, Woźniak 2000; Alard & Lupton 1998). Photometric databases were created for both pass-bands as described in Szymański (2005) and are available on-line¹.

The OGLE–II observations of the LMC began in December 1996 (HJD=2450446), but during the first year only the very central fields (i.e. those that are, in general, denser) were observed (fields 1–10 and 12). In November 1997 (HJD=2450726), fields 11 and 13–20 were added to the observing queue, and the addition of the field LMC_SC21 in January 1998 (HJD=2450831) eventually formed the entire set of OGLE–II fields. All 21 fields were monitored continuously until November 2000 (HJD=2451874), yielding about 500 and 300 frames per field in the *I* band for dense and sparse fields, respectively. In the *V* band, there were no more than 50 frames per field collected in total during the duration of the project. On average, each field was observed every third night in the *I* band, and every 11-th night in the *V* band. Mean seeing was 1.35 arcsec in the *I* and 1.37 arcsec in *V*. Template images were created by stacking the best seeing images, resulting in images with seeing of about 1.1 arcsec. The template images contained about 5.5 million objects suitable for our study in the *I* and *V* band.

The detection of microlensing events and the efficiency determination have been performed using *I*–band data only, as these were far more numerous and were sampled more frequently as compared to *V*–band photometry.

In this study we also occasionally made use of OGLE–III LMC data from years 2001–2008, which covered a much wider area and included the OGLE–II fields. Details of the instrumentation and photometric pipeline can be found in Udalski (2003). Analysis of OGLE–III LMC data will be presented separately in a forthcoming paper (Wyrzykowski et al., in preparation).

Additionally, for the two detected events, we also use the data gathered by the MACHO group and provided on their WWW interface². The reductions of the images and extraction of the photometry were performed with Difference Image Analysis following Kozłowski et al. (2007).

3 ERROR-BARS CORRECTION

Photometric error bars calculated using the Difference Image Analysis method are known to be generally underestimated. This effect is most pronounced for bright stars, as

¹ <http://ogledb.astrow.edu.pl>

² <http://wwwmacho.mcmaster.ca/Data/MachoData.html>

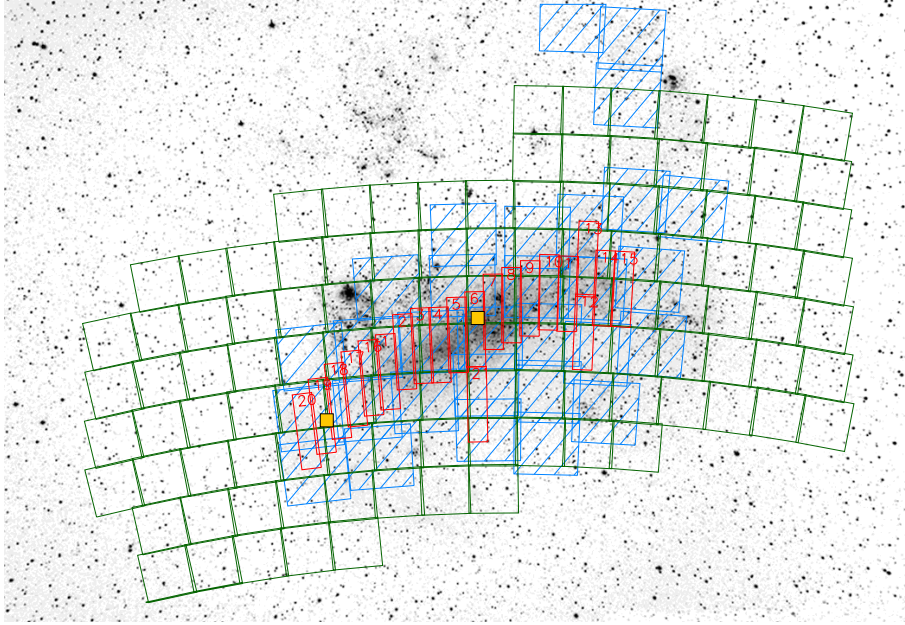


Figure 1. Positions of the OGLE-II LMC fields (red rectangles with labels). Also shown are all OGLE-III (green squares) and MACHO project fields (blue dashed squares). EROS fields are not shown here as they cover nearly the whole picture. The two small gold-filled squares show the positions of the HST fields used for our blending determination. Background image credit: Peter Ward.

Table 1. The OGLE-II LMC fields.

Field	RA_{J2000}	Dec_{J2000}	No of stars		Stellar density	Density level
			template	estimated real	[stars/sq.arcmin]	
LMC_SC1	5:33:48.84	-70:06:07.9	288029	668799	367	dense
LMC_SC2	5:31:17.17	-69:51:57.0	332267	771301	424	dense
LMC_SC3	5:28:47.95	-69:48:05.6	355075	822913	453	dense
LMC_SC4	5:26:17.82	-69:48:06.1	390484	904432	498	dense
LMC_SC5	5:23:47.79	-69:41:03.3	379709	878472	484	dense
LMC_SC6	5:21:18.34	-69:37:10.3	392781	909775	501	dense
LMC_SC7	5:18:48.01	-69:24:09.9	388918	900339	496	dense
LMC_SC8	5:16:17.91	-69:19:13.7	349202	807890	445	dense
LMC_SC9	5:13:47.92	-69:14:05.8	289391	671459	369	dense
LMC_SC10	5:11:16.10	-69:09:17.3	258706	599375	330	dense
LMC_SC11	5:08:41.06	-69:10:03.1	253395	588432	323	dense
LMC_SC12	5:06:16.15	-69:38:18.3	186951	318893	238	sparse
LMC_SC13	5:06:14.18	-68:43:30.3	214229	365917	273	sparse
LMC_SC14	5:03:48.62	-69:04:44.3	222569	380394	284	sparse
LMC_SC15	5:01:17.27	-69:04:42.9	170657	291859	218	sparse
LMC_SC16	5:36:17.62	-70:09:41.9	247981	575953	316	dense
LMC_SC17	5:38:47.47	-70:16:44.1	194661	332187	248	sparse
LMC_SC18	5:41:17.77	-70:24:48.0	166998	285126	213	sparse
LMC_SC19	5:43:47.91	-70:34:42.7	156353	267126	199	sparse
LMC_SC20	5:46:17.85	-70:44:50.0	152186	260515	194	sparse
LMC_SC21	5:21:13.73	-70:33:18.7	143979	244667	184	sparse
total			5534521	11845824		

Coordinates point to the centre of the field, each being $14' \times 56'$. The number of 'good' objects in the template is provided (number of data points > 80 and mean I -band magnitude < 20.4 mag) together with the estimated number of real monitored stars (see Section 6). Stellar density in number of stars per square arc minute was used to classify fields into *dense* or *sparse* classes with the threshold of 300 stars/sq.arcmin.

Table 2. Error correction coefficients for OGLE–II LMC fields.

Field	γ	ϵ
LMC_SC1	1.327934	0.002309
LMC_SC2	1.534320	0.000000
LMC_SC3	1.514598	0.000000
LMC_SC4	1.534963	0.000000
LMC_SC5	1.552337	0.000000
LMC_SC6	1.512235	0.000000
LMC_SC7	1.546070	0.000000
LMC_SC8	1.376516	0.001565
LMC_SC9	1.432857	0.001066
LMC_SC10	1.306555	0.001539
LMC_SC11	1.084232	0.002695
LMC_SC12	1.325315	0.001657
LMC_SC13	1.369874	0.001256
LMC_SC14	0.932450	0.002931
LMC_SC15	1.168966	0.002046
LMC_SC16	1.151916	0.002628
LMC_SC17	1.149929	0.002365
LMC_SC18	1.205946	0.002624
LMC_SC19	1.128117	0.003138
LMC_SC20	1.203747	0.002623
LMC_SC21	1.301942	0.002467

noted already by the authors of the DIA method (Alard & Lupton 1998). In microlensing studies this affects the brightest parts of events, increasing the χ^2 values in microlensing model fitting. In order to increase the detectability of events, we derived and applied an error bar correction factor.

Typically, error bars in microlensing surveys are corrected by calculating one single correction factor for an entire light curve, derived at the event’s baseline (assuming the baseline is constant). This approach, however, does not account for the need for varying correction factors for different apparent magnitudes, which in case of highly magnified events leaves the error bars at the peak of the event significantly underestimated. Also, as shown in Wyrzykowski et al. (2006), some events exhibit intrinsic variability in their baselines due to variability of the microlensed source or one of the blended stars, in which case the derived photometric error bars are overestimated.

In this study, we processed the entire OGLE–II data set and determined the correction coefficients in an empirical way. For each OGLE–II field, we extracted the I -band light curves of stars and compared their intrinsic error-weighted rms with the mean error returned by the photometry pipeline. In order to produce statistically comparable results, in each light curve we selected only the first 250 measurements for further analysis, as different fields had different numbers of frames taken. In the plot of rms vs magnitude (see Fig. 2), the lowest boundary of the rms is occupied by the least variable (i.e., constant) stars. On the other hand, the lowest outline of mean error bar is defined by the errors assigned to the best measurements at given magnitude. In an ideal situation these two curves should follow each other, i.e., every constant star should have its rms equal to its mean error bar. As can be seen from the upper panel of Fig. 2, for our data the mean errors were systematically lower than the rms .

In order to account for this systematic shift we have fitted the following two-parameter formula which minimised

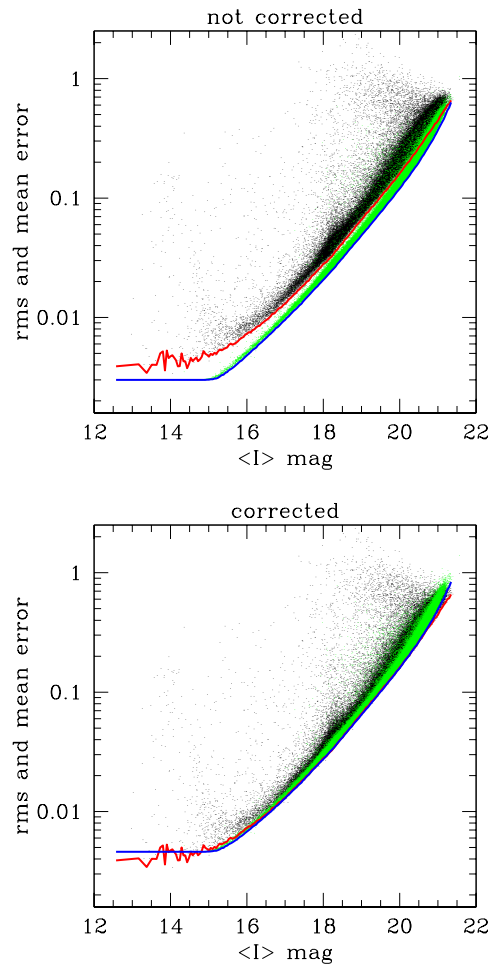


Figure 2. Mean error (green) and rms (black) for a sample of stars from OGLE–II LMC_SC1 field before (upper panel) and after (lower panel) the correction of error bars. Lines indicate the lower outlines of the rms (red) and mean error bar (blue).

the difference between lower outlines of the rms and mean error bars:

$$\Delta I_{cor} = \sqrt{(\gamma \Delta I)^2 + \epsilon^2}, \quad (1)$$

where ΔI is the error bar returned by the photometry pipeline, γ and ϵ are the correction coefficients and ΔI_{cor} is the corrected error bar.

The lower panel of Fig.2 shows the rms and mean error bars after applying the corrections to each light curve’s individual error bar measurements using Equation 1.

Table 2 presents γ and ϵ coefficients derived for each OGLE–II LMC field. The mean γ and ϵ for all LMC fields were 1.32 and 0.0016, respectively. Derived correction coefficients are suitable for use in any study involving OGLE–II Large Magellanic Cloud photometric data.

As a by-product of the error bar analysis we derived the formula for scaling real error bars from some reference light curve to any magnitude, which is necessary for the simulation of light curves:

$$\begin{aligned} \Delta I_{sim} &= \Delta I_{ref} 10^{0.35(I_{sim} - I_{ref})}, & \text{for } I_{sim} \geq 15.0 \\ \Delta I_{sim} &= 0.003, & \text{for } I_{sim} < 15.0, \end{aligned} \quad (2)$$

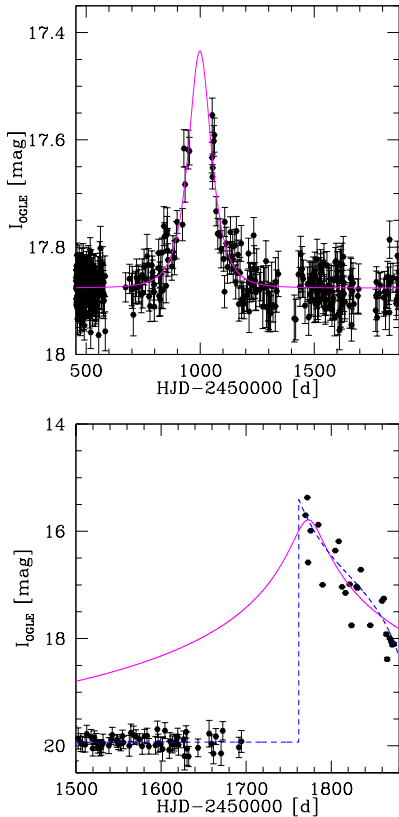


Figure 3. Two sample light-curves for false-positive events, which were rejected in the search procedure. Top: “blue bumper” (which exhibited a second bump in the OGLE-III data). Bottom: possible nova or supernova with additional variability in the declining part. Solid magenta line is the best microlensing model, dashed blue line is a nova model.

where I_{sim} is the simulated magnitude for which the error bar (ΔI_{sim}) is required, I_{ref} and ΔI_{ref} are the magnitude and the error bar of the reference star at a given epoch. These error bars still need to be corrected using eq. (1).

4 SEARCH PROCEDURE

We searched for microlensing events among 5.5 million objects, selected from the database as having more than 80 data points and mean magnitude in I band brighter than 20.4 mag (cut 0). This defined our All Stars Sample. All light curves now have their measurements’ error bars corrected as described in Section 3.

Table 3 presents all of the cuts, along with the number of objects left after each cut. All parameters for this procedure were derived and fine-tuned for OGLE-II LMC data after carrying-out Monte Carlo simulations of microlensing events, using the simulation procedures described in Section 7.

The first step of the search procedure is similar to the one used in the search for microlensing events in the OGLE-II Galactic bulge data (Sumi et al. 2006). All objects were searched for a bump over a baseline, allowing for some variability in the baseline.

For a given light curve, we introduce an outer window

with width equal to half of the total observational time-span. The significance of each data point σ_i with respect to the outer window was calculated via

$$\sigma_i = \frac{I_{\text{med},w} - I_i}{\sqrt{\Delta I_i^2 + \sigma_w^2}} \quad (3)$$

where I_i is the magnitude of the point i and ΔI_i is its error bar, while $I_{\text{med},w}$ and σ_w are the median and the *rms* in the outer window, respectively. The bump was detected when there were at least 4 consecutive data points above a $\sigma > 1.4$ threshold and 3 of them were above a $\sigma > 2.5$ threshold. Up to 2 peaks were allowed in one light curve, but then only the one with the highest σ_{max} was chosen. If the sum of σ s over the peak data points was higher than 30.0 the light curve was selected (cut 1).

In cut 2, we masked out possible “blue bumpers” (Alcock et al. 2000b) – variable stars located on the bright blue part of the Main Sequence, exhibiting outbursts that can look similar to the microlensing phenomenon. The upper panel of Fig. 3 shows an example of a “blue bumper” star, rejected due to its magnitude and colour. This particular object also exhibited additional significant variation in the OGLE-III data in subsequent years.

In the next step, the remaining light curves were fitted with the standard Paczyński (1996) microlensing model, (i.e., a point-source – point-lens microlensing event) which is described as:

$$I = I_0 - 2.5 \log [f_S A + (1 - f_S)], \quad (4)$$

where

$$A = \frac{u^2 + 2}{u\sqrt{u^2 + 4}} \quad \text{and} \quad u = \sqrt{u_0^2 + \frac{(t - t_0)^2}{t_E^2}}. \quad (5)$$

The fitted parameters are: t_0 – the time of the maximum of the peak, t_E – the Einstein radius crossing time (event’s time-scale), u_0 – the event’s impact parameter, I_0 – the baseline magnitude in the I band and f_S – the blending fraction (ratio of lensed source flux to total blends’ flux in the I band). The fits were performed in two ways, namely with blending parameter fixed $f_S = 1$, i.e., with no blending, and with f_S being free. For clarity, parameters of the non-blended (4 parameters) model are given the subscript $\mu 4$.

Then we compared the 4-parameter microlensing model (with blending fixed to 1 to assure convergence) with a constant line fit (cut 3). A similar cut was also applied in the EROS analysis (Tisserand et al. 2007), where it proved to be very efficient. $N_{\text{dof},\mu 4}$ and $N_{\text{dof},\mu 4,\text{peak}}$ are the degrees of freedom of the fit calculated using numbers of data points in the entire light curve and around the peak, respectively. This cut removed many low signal-to-noise bumps and allowed us to select only the outstanding bumps.

In cut 4, we required that there were more than 6 data points around the microlensing peak in the range of $t_0 \pm t_{E\mu 4}$. This meant that we had enough data points in the bump to analyse.

Next we attempted to remove all plausible novae, supernovae and all kinds of asymmetric bumps contaminating our sample (cut 5). We fitted the light curves with an general asymmetric model, following the formula used for the novae search in e.g. Feeney et al. (2005), which comprises of two scalable exponents and a constant baseline. We com-

Table 3. Selection criteria for microlensing events in the OGLE-II data

Cut no.			No. of objects left
0	Selection of “good” objects	$N > 80, \langle I \rangle \leq 20.4 \text{ mag}$	5,534,521
1	Significant bump over baseline	$\sum_{peak} \sigma_i > 30.0$	9,390
2	“Bumper” cut [†]	$\langle I \rangle > 19.0 \text{ mag}, \langle V - I \rangle > 0.5 \text{ mag}$	7,867
3	Microlensing fit better than constant line fit	$\frac{\chi_{ine}^2 - \chi_{\mu 4}^2}{\frac{\chi_{\mu 4}^2}{N_{dof, \mu 4}} \sqrt{2N_{dof, \mu 4, peak}}} > 140$	1,020
4	Number of points at the peak*	$N_{peak} > 6$	968
5	Microlensing fit better than supernova fit,	$\chi_{SN}^2 > MIN(\chi^2, \chi_{\mu 4}^2)$	607
6	Peak within the data span [HJD-2450000]	$446 \leq t_0 \leq 1874$	591
7	Blended fit converged	$0 < f_S < 1.2$	113
8	Conditions on goodness of microlensing fit (global and at the peak)	$\frac{\chi^2}{N_{dof}} \leq 2.3$ and $\frac{\chi_{\mu 4, peak}^2}{N_{dof, \mu 4, peak}} \leq 5$	4
9	Time-scale cut [<i>d</i>]	$1 \leq t_E \leq 500$	2
10	Impact parameter cut	$0 < u_0 \leq 1$	2

[†] magnitudes as in the field LMC_SC1 (shifted according to the position of the center of Red Clump)

*in the range of $t_0 \pm t_{E\mu 4}$

pared its goodness-of-fit with the χ^2 of microlensing model, taking the smaller of blended and non-blended fits. This cut was sensitive to all sorts of asymmetric light curves. Among the removed objects were several dwarf novae candidates, as well as long-term varying objects and several eruptive Be stars. These Be stars were fainter or redder than our Blue Bumper cut and typically exhibited a flat baseline, a sharp rise and a slow decline (e.g., Keller et al. 2002).

Assuming a supernova rate of $0.5 \text{ SNe yr}^{-1} \text{ deg}^{-2}$ above $V = 20 \text{ mag}$ (Alcock et al. 2000b), then for our experiment of 4 years covering 4.5 square degrees and assuming detection efficiency of about 20 per cent we should expect about 1 supernova in our data set. Visual inspection of the light curves rejected at the supernova fit stage (cut 5) indeed showed one plausible candidate for a supernova (see lower plot of Figure 3).

In the following step (cut 6), we removed all light curves in which the peak occurred before the beginning or after the end of the time-span of the OGLE-II observations.

Next, in cut 7 we selected only those candidates whose blended microlensing fit has converged with blending parameter $f_S < 1.2$. We allowed for small amount of ‘negative’ blending following previous studies (e.g., Park et al. 2004, Smith et al. 2007) showing regular event can be affected by this effect. The vast majority of the light curves removed in cut 7 had f_S significantly larger than 2, indicating that the blending fit did not converge.

In cut 8, we requested the reduced χ^2 of the blended microlensing fit was less than 2.3 and the χ^2 of the non-

blended model calculated on the peak only (within $1 t_{E\mu 4}$ around t_0) was less than 5.0. This stage removed obvious variable stars with a single bump lying above the rest of the light curve to which the microlensing model was fit quite poorly. We were able to apply this cut uniformly to all light curves, independently on their magnitude, thanks to the fact that the error bars were corrected and any dependence on the measurement brightness was accounted for (Section 3).

The final cuts 9 and 10 are applied to select candidates suitable for the optical depth determination. For this, we used microlensing parameters obtained with the fitting procedure, and required the time-scales t_E to be between 1 and 500 days and impact parameter u_0 less than 1 Einstein radius.

5 RESULTS

Out of 5.5×10^6 light curves we found only two plausible candidates for microlensing events. These are labeled OGLE-LMC-01 and OGLE-LMC-02.

Table 4 presents their coordinates, OGLE-II field, star id, baseline *I*- and *V*-band magnitudes obtained in the microlensing fit and magnitude and colour of the source.

Both candidate light curves were checked for available additional data outside the time-span of the OGLE-II project. We cross-correlated them with the OGLE-III database, covering years 2001–2008 (the most-recent data used were obtained in May 2008) and the MACHO database,

Table 4. Microlensing candidates detected in the OGLE-II LMC data.

Event's name	RA [J2000.0]	Dec [J2000.0]	field	database star id	baseline <i>I</i> [mag]	baseline <i>V</i> [mag]	source <i>I</i> [mag]	source <i>V</i> − <i>I</i> [mag]
OGLE-LMC-01 (EWS: OGLE-1999-LMC-01) (MACHO-99-LMC-2)	5:16:53.26	-69:16:30.1	LMC_SC8	235928	19.91 ±0.01	20.65 ±0.14	19.90 ±0.06	0.887* ±0.007
OGLE-LMC-02	5:30:48.00	-69:54:33.6	LMC_SC2	170259	20.42 ±0.02	20.68 ±0.13	20.53 ±0.38	0.46 ±0.03

* colour derived using MACHO *B*-band data

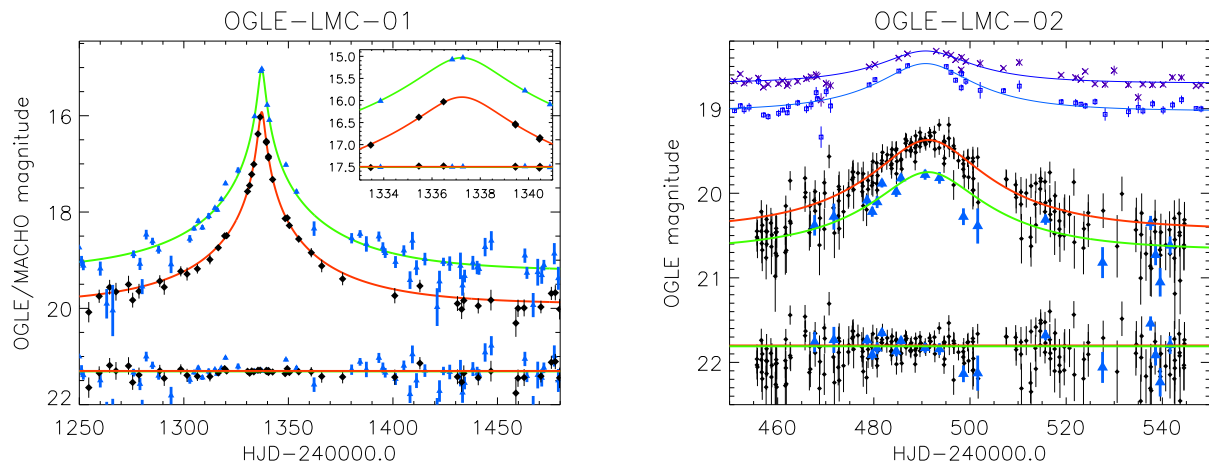


Figure 4. Light curves of the two OGLE-II events OGLE-LMC-01 (left panel) and OGLE-LMC-02 (right panel). Black points are the OGLE *I* band, blue triangles are the MACHO *B*-band and OGLE *V*-band observations, for OGLE-LMC-01 and OGLE-LMC-02, respectively. Solid red and green lines show the best-fitting microlensing models to the data, with residuals shown below each curve. The inset shows a zoom-in around the peak of amplification, indicating that the finite-source effect is not detectable. Re-reduced MACHO data and the fit for OGLE-LMC-02 are shown above the OGLE data shifted by 0.5 mag (squares for *B*, crosses for *R*).

covering years 1992–1999, yielding total data coverage of 16 years. Neither candidate exhibits additional variability apart from the actual event.

In the OGLE-II database there were 44 *V*-band observations of OGLE-LMC-01, but none of them were taken during the event. Therefore for colour determination of the source, we used re-reduced MACHO data in the *B* band. By comparing the OGLE *V* and *I* CMD with MACHO *B*-band photometry of nearby stars, we found the following transformation for the colour: $(B-I) = (1.1571 \pm 0.0046)(V-I) + const$, where the measured constant is an artefact of the instrumental magnitude system of our reductions of the MACHO data. For OGLE-LMC-02, we used the OGLE *V*-band data, as there were 59 observations available, with about 14 taken during the peak.

Close-ups of the events are shown in Fig. 4 along with the best-fitting microlensing models and their residuals.

The top panel of Fig. 5 shows the colour-magnitude diagram of LMC stars based on OGLE and HST (Holtzman et al. 2006) data, along with the determined positions of the sources in the two OGLE candidates. For comparison, we have also included in this figure the candidates from the MACHO collaboration: different colours and shapes differentiate between self-lensing candidates according to Mancini et al. (2004), the binary event MACHO-LMC-9, the thick disk

lens candidates MACHO-LMC-5 (Kallivayalil et al. 2004) and MACHO-LMC-20 (Kallivayalil et al. 2006) and the remaining candidates.

In the bottom panel of Fig. 5, the positions of OGLE-II and MACHO candidates are shown on the map of stellar density of the Red Clump stars from the OGLE-III data.

5.1 OGLE-LMC-01

This was the only event detected towards the LMC by the Early Warning System (EWS, Udalski et al. 1994) during the entire second phase of the OGLE project and was designated OGLE-1999-LMC-01³. It was also independently discovered and alerted by the MACHO collaboration (MACHO-99-LMC-02), but it was not included in Alcock et al. (2000b) as it occurred outside the 5.7 year time-span of analysed data (MACHO star ID: 79.5863.4522, see also Bond et al. 2002).

The OGLE-II data were fitted with the standard Paczyński microlensing model, i.e., a point-source–point-lens model (eq. 4). When we fixed blending such that the event

³ <http://www.astrouw.edu.pl/~ogle/ogle2/ews/1999/lmc-01.html>

Table 5. Parameters of the microlensing model fits to the OGLE-LMC-01 and OGLE-LMC-02 events.

OGLE-LMC-01						
parameter	5-parameter fit		4-parameter fit		7-parameter fit	
t_0	1337.20	± 0.02	1337.20	± 0.02	1337.20	± 0.01
t_E	57.2	$^{+4.7}_{-4.2}$	59.2	± 0.7	65.7	± 2.6
u_0	0.0258	$^{+0.0024}_{-0.0023}$	0.0248	± 0.0004	0.0231	± 0.0009
I_0	19.91	± 0.01	19.91	± 0.01	19.92	± 0.01
f_{S_I}	1.04	± 0.09	1.0	—	0.91	± 0.04
B_0	—	—	—	—	18.28	± 0.01
f_{S_B}	—	—	—	—	1.11	± 0.05
χ^2	286.7		286.9		3401.0	
$\frac{\chi^2}{N_{dof}}$	0.88		0.87		2.68	
OGLE-LMC-02						
parameter	5-parameter fit		4-parameter fit		7-parameter fit	
t_0	491.6	± 0.3	491.6	± 0.3	491.3	± 0.3
t_E	23.8	$^{+6.0}_{-5.1}$	24.2	± 1.0	27.4	$^{+6.9}_{-5.6}$
u_0	0.4120	$^{+0.1856}_{-0.1164}$	0.4011	$^{+0.0083}_{-0.0081}$	0.3478	$^{+0.1428}_{-0.0955}$
I_0	20.42	± 0.02	20.42	± 0.02	20.44	± 0.02
f_{S_I}	1.04	$^{+0.77}_{-0.37}$	1.0	—	0.83	$^{+0.52}_{-0.28}$
V_0	—	—	—	—	20.68	± 0.02
f_{S_V}	—	—	—	—	0.67	$^{+0.42}_{-0.22}$
χ^2	578.2		578.2		636.2	
$\frac{\chi^2}{N_{dof}}$	1.21		1.20		1.19	

was unblended ($f_{S\mu 4} = 1$) we obtained $t_{E\mu 4} = 59.2 \pm 0.7$ days, whilst when f_S was free, we found $t_E = 57.2^{+4.7}_{-4.2}$ days ($f_S = 1.04 \pm 0.09$). When OGLE I - and MACHO B -band data were fitted simultaneously, the derived timescale was somewhat larger ($t_{EVI} = 65.7$ days), as the blending parameter in I -band changed slightly. The results of the fits are summarised in Table 5.

Since the event was relatively long we checked if OGLE-LMC-01 was subject to the parallax effect (e.g., Han & Gould 1995b). The components of the parallax vector π_E in the OGLE-II data fit were $\pi_{E,N} = -0.03 \pm 0.10$ and $\pi_{E,E} = -0.16 \pm 0.25$, i.e., consistent at 1- σ level with no detection of parallax (Gould 2004). Therefore, the time-scale derived in the fit is not subject to any degeneracy with parallax. In principle the lack of parallax signatures allows us to place limits on lens distance. However, for this event the parallax constraints are not very tight and so the limits are not particularly insightful: if we assume that the source lies at the distance of the LMC (~ 50 kpc) and the lens is $0.5M_\odot$,

we find that the 2-sigma lower-limit on the lens distance is 300 pc. From this, we cannot make any significant statements about the population to which the lens belongs.

With a maximum amplification of about 40 (~ 4 mag), this is one of the most secure and best constrained events towards the LMC found to date. High amplification events are often prone to exhibit finite-source effects in cases where the source and the lens are close to each other. We checked for the presence of this effect in the OGLE and MACHO data. In particular, MACHO data had two observations very close to the peak, where the effect should be most pronounced. We have not detected any deviation (see inset in Fig. 4). This only allows us to put an upper limit on the source star size in units of the Einstein radii of $\rho > 0.0332$, which along with an estimation of the source size ($\theta_* = 0.42 \mu\text{as}$) lead to an upper limit on $\theta_E = \theta_*/\rho > 13.1 \mu\text{as}$. This at the LMC distance is equivalent to about 0.66 AU. Hence, the limit on the projected transverse velocity of the lensing object

$v_{\perp} = \theta_E/t_E > 21$ km/s, which is satisfied by typical lenses in both the LMC and Galaxy halo.

A simultaneous microlensing model fit to the OGLE I -band and MACHO B -band data gives an apparent source magnitude of $I_s = 19.90 \pm 0.06$ and colour $(V-I)_s = 0.887 \pm 0.007$. Magnitudes and location of the source on the CMD in Fig. 5 indicate it belongs to the Red Giants Branch of the LMC.

5.2 OGLE-LMC-02

The second event, OGLE-LMC-02, was found just at the limit of our magnitude cut (the actual mean brightness was 20.29 mag, which means that it passed cut 0). The maximum amplification of ~ 2.6 produced a rise in brightness of ~ 1 mag. This event occurred in the very first season of the LMC observations in the OGLE-II, when the sampling was much denser than in subsequent seasons. Therefore, the microlensing light curve was very well covered and prominent (see Fig. 4).

Again, we used the standard point-source-point-lens model to fit the OGLE-II data. The unblended fit ($f_{S\mu 4} = 1$) gave a time-scale $t_{E\mu 4} = 24.2 \pm 1.0$ days, and for unconstrained f_S we found $t_E = 23.8_{-5.1}^{+6.0}$ days ($f_S = 1.04_{-0.37}^{+0.77}$). The large error bars in f_S and t_E were also present in the simultaneous fit to I - and V -band observations, which yielded a time scale of $t_{E_{IV}} = 27.4$ days.

This object was also observed by the MACHO collaboration (MACHO star ID: 77.8152.2917). However, the event was not detected by them, probably due to noisy data and sparse sampling. The peak was clearly revealed in both red and blue filters only after DIA re-reductions of the original MACHO images and its best-fitting microlensing model had a time-scale of around 25 days, consistent with the fit to the OGLE data.

From the fit to the two-band OGLE data, we derived the magnitude and colour of the lensed source. The position of the source with magnitude $I_S = 20.53 \pm 0.38$ and colour $(V-I)_S = 0.46 \pm 0.03$, is marked on the Fig. 5 and indicates it is probably a Main Sequence star located in the LMC.

Its location on the Main Sequence branch of the CMD means that this may potentially be a candidate for a blue bumper. However, while many blue bumpers exhibit secondary brightening episodes, the baseline of this event proved to be constant over more than 15 years. Therefore, we believe that it is unlikely to be a blue bumper.

6 BLENDING AND NUMBER OF MONITORED STARS

Microlensing collaborations have deliberately chosen to monitor the densest fields on the sky, namely the Galactic Center and Magellanic Clouds. This is done in order to increase the number of potentially detectable microlensing events, as the chances of seeing an events are of the order of 10^{-7} (i.e., one out of 10 million monitored stars is undergoing a microlensing episode at any given time). However, in such crowded stellar fields observed with a medium-sized ground-based telescope, virtually every object detected on the image consists of several stars blended together. Neglecting blending can have severe consequences on the optical

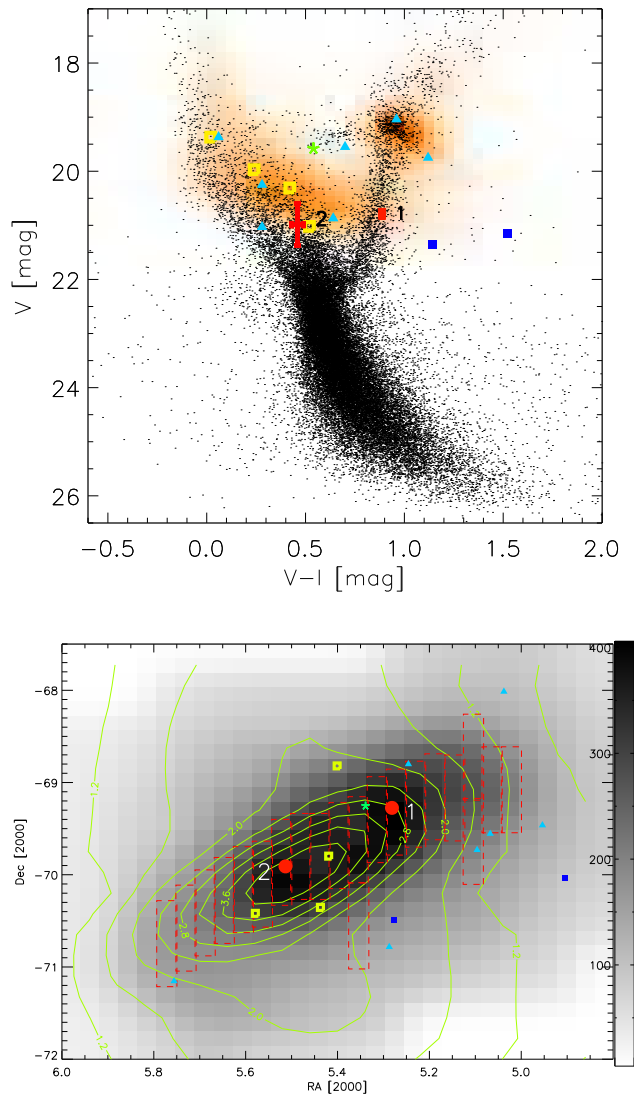


Figure 5. CMD of OGLE-II and MACHO candidate microlensing events, overplotted on the OGLE (red background) and HST (black dots) measurements of stars in central parts of the LMC (upper panel). Positions of OGLE and MACHO candidate events on the OGLE-III LMC Red Clump star count map (lower panel). The contours show modelled self-lensing optical depth from Mancini et al. (2004) and run every 0.4×10^{-8} with 4×10^{-8} at the innermost one. Dashed boxes mark OGLE-II fields. Positions of the sources in the two OGLE events are marked in red and with a number. Remaining symbols represent MACHO candidates with binary event #9 (green star), candidates for self-lensing (yellow squares), confirmed thick-disk lenses #5 and #20 (dark blue filled squares) and remaining marked with blue triangles.

depth measurements (e.g., Sumi et al. 2006), as the amplifications and time-scales of microlensing events may be determined incorrectly, sometimes by a factor of 2 or more. On the other hand, Smith et al. (2007) showed that in the case of the Galactic bulge the effect of overestimation of the events' time-scales cancels out with the underestimate of the real number of monitored stars to lowest order.

Dealing with blending is a delicate and difficult task.

Adding a blending parameter to the standard microlensing light curve model may cause degeneracies in the parameter space of the microlensing events (e.g., Woźniak & Paczyński 1997). Therefore, the favoured approach in recent optical depth determinations towards the Galactic bulge and Magellanic Clouds is to neglect blending by narrowing the star sample to the brightest stars only (Popowski et al. 2005, Tisserand et al. 2007). However, in the case of Magellanic Clouds the number of possible events is very small and it is even more unlikely to detect a microlensing event occurring in the limited number of bright stars.

In our analysis, we decided to use all stars available in the OGLE-II database. To deal with the blending issue – which is most serious for faint stars – we make use of the archival images from the Hubble Space Telescope (HST)⁴ located by chance in our fields. The HST images have superior resolution when compared to the ground-based OGLE images (i.e. they are nearly blending-free) and are usually much deeper than the OGLE data. Therefore these data are a valuable source of information regarding the amount of blending. In the HST archive, we identified two deep ACS *I*-band images coinciding with the OGLE fields, located in OGLE fields LMC_SC6 and LMC_SC19, as typical representatives of the dense and sparse parts of the LMC. The location of these fields is shown in Fig. 1.

The positions of the HST stars were transformed onto the OGLE images and then we identified which HST stars contributed to each OGLE object by calculating their distances from the OGLE blend’s centre. A blend’s radius was estimated using the Gaussian profile for the given blend’s magnitude at a chosen level above the background ($I \simeq 19.7$ mag) with an additional 1.3 pixel added in quadrature. We identified HST stars that were not more than 3.5 mag fainter than the OGLE blend (i.e., $f_s > 4$ per cent) and considered stars located within the blend radius as components of that blend. This method allowed us to create an empirical distribution of the blending fractions for dense and sparse fields. We divided these distributions into three magnitude bins: $14 \text{ mag} < I \leq 17.5 \text{ mag}$, $17.5 \text{ mag} < I \leq 19 \text{ mag}$ and $19 \text{ mag} < I \leq 20.4 \text{ mag}$. They are shown in Fig. 6.

Then, every OGLE LMC field was classified as dense or sparse according to its average stellar density down to 20.4 mag (with 300 stars per square arcmin as a division boundary) on the OGLE template image (see Table 1). We then adopted the corresponding distributions in the detection efficiency calculations and in our recalculation of the number of monitored stars (see Section 7).

Due to blending in ground-based observations, we can not resolve individual stars that are separated by less than the typical seeing (of order of 1 arcsec). Even though the OGLE template images, with respect to the typical images, have usually high resolution thanks to stacking of \sim a dozen of the best-seeing images, we still have limited ability to resolve individual stars. Since each OGLE template object may consist of several stars, any of which could be microlensed, the number of stars we consider as potential sources for microlensing events is actually larger than number of objects detected on the template image.

In order to estimate the actual number of monitored

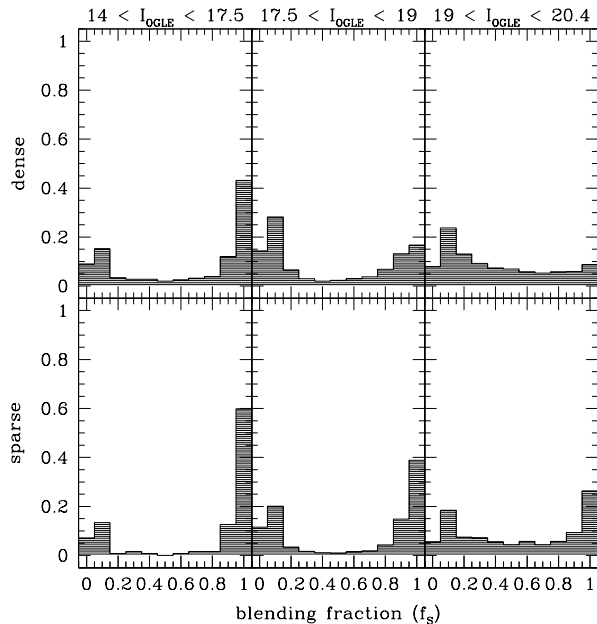


Figure 6. Distributions of blending fractions for stars from the analysis of the archival high-resolution HST images of parts of the OGLE fields.

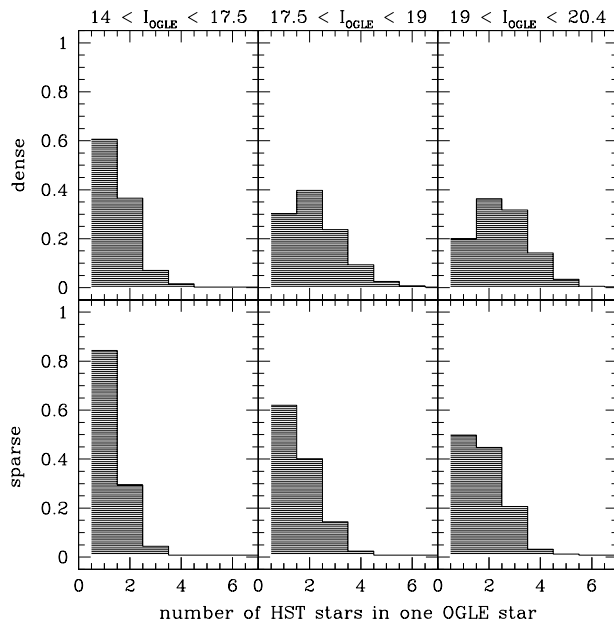


Figure 7. Distribution of the number of HST stars in one OGLE-II object obtained for dense and sparse fields.

stars – which enters directly into eq. (6) – we derived the distributions of the number of HST stars hidden in a single OGLE template object (see Fig. 7) using the same HST images and photometry. Then, for each OGLE field we convolved its luminosity function with the distribution in each magnitude bin (for a corresponding density level). The estimated numbers of monitored stars in each field are provided in Table 1. On average, the correction factor for dense fields

⁴ <http://archive.stsci.edu/hst/>

was about 2.3 and for sparse about 1.7. The total number of monitored stars was estimated to be about 11.8 million, compared to about 5.5 million objects detected on the OGLE-II template images in cut 0.

It is worth pointing out that in our method of counting the total number of monitored stars we did not count all stars that would be observed with the HST down to 23.9 mag (20.4 mag + 3.5 mag). We counted only those stars which were blended with other stars such that they formed a blend of magnitude brighter than 20.4 mag on the OGLE template image. For instance, a single 21 mag star might not be detected on the template image. Even if microlensed, we would not detect this event as in our analysis we did not search for transient events with no baseline (i.e., with no object on the template). If such star, however, was blended with another 21 mag star they would form a 20.2 mag object – very likely detectable on the template. In this case, both components would have blending factor of $f_S = 0.5$ and both of them would be counted as a separate potential source for microlensing events.

7 DETECTION EFFICIENCY

The task of calculating the detection efficiency for microlensing events can be a complicated procedure. In general, this requires us to simulate events and then determine the fraction that we recover with our selection criteria. It may seem that the most accurate method is to inject microlensing events into the series of real frames or to create completely new mock images and then put them through the entire photometric pipeline. However, this is obviously very intensive computationally. Furthermore, it is not clear how to deal with the fact that any star within the blended object can be microlensed or whether the mock frame is indeed reproducing all characteristics of the real one.

Some of these problems can be also encountered when simulating microlensing events at the so-called ‘catalogue-level’ (which only involves generating series of light curves). However, the computational effort required for this procedure is significantly reduced and some difficulties can be resolved more easily.

The ‘image-level’ simulations were performed by MACHO and MOA collaborations in their calculation of the optical depth towards the Galactic bulge (Alcock et al. 2000a; Sumi et al. 2003; Alcock et al. 2001). The ‘catalogue-level’ approach has been more commonly used for the bulge (e.g., Afonso et al. 2003; Hamadache et al. 2006; Sumi et al. 2006) and in the EROS collaboration’s study of microlensing towards the Magellanic Clouds (Tisserand et al. 2007).

In this study, we decided to use the existing photometric light curves as a base for the simulations. However, as we discuss below, we have attempted to incorporate all of the advantages of the ‘image-level’ simulations. As shown in Kozłowski (2007) such an approach can be very successful when all factors are carefully taken into account.

The detection efficiency was determined individually for the fields containing both events (SC2 and SC8). For a wide range of time-scales between 1 and 1000 days, we performed Monte Carlo simulation of about 10^5 events. From the field’s photometric database, a star was picked randomly, provided that the star satisfied the basic cut 0 (i.e., it had the required

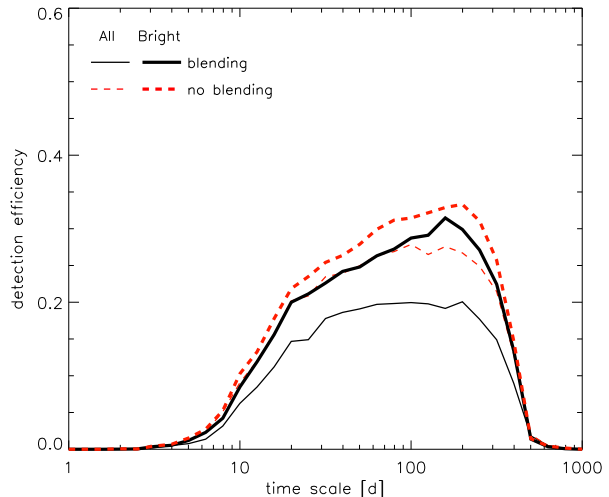


Figure 8. Detection efficiencies for OGLE-II LMC_SC8 field for All (thin lines) and Bright (thick lines) Stars Samples, with blending included (solid lines) and neglected (dashed lines). For most of the dense fields, the detection efficiencies follow these relations. The efficiencies for the most of the sparse fields are lower by a about 30 per cent due to the fact they have a shorter time-span of observations.

number of data points and sufficient mean brightness). For a given t_E , the other microlensing parameters were drawn from flat distributions (t_0 and u_0) and from the empirically derived distributions for the blending parameter (f_S ; see Section 6). The latter was chosen with respect to the stellar density level of the simulated field and the magnitude bin in which the simulated star was located. The original flux of the input star was apportioned between the source and blend in the ratio $f_S : 1 - f_S$.

Effectively, the lensed flux was added to already existing stars in the database, so no new stars were ‘created’. Also, the procedure preserved any variability and non-gaussianity present in the original photometry, allowing for effects of decreasing or increasing of the variability amplitude during microlensing (Wyrzykowski et al. 2006). Photometric error-bars were scaled according to the empirically derived relation between the error bars and the magnitude (see eq. 3). Such simulated events were then analysed with our search pipeline described in Section 4.

In their LMC data, the MACHO collaboration found one event (MACHO-LMC-9) to be a clear caustic crossing binary lens. Our detection pipeline discriminated against binary and other exotic events, as we only fitted a point-source–point-lens microlensing model. However, we performed a visual inspection of the several thousands of high signal-to-noise light curves that passed cut 1, and found no candidates for any non-standard type of events. Our detection efficiency did not take into account the influence of binary lenses because Monte Carlo simulations of binary events and their automated recovery is a difficult and computationally demanding task. Therefore we followed the approach adopted by the EROS group (Tisserand et al. 2007) and reduced the efficiency by a factor of 0.9 to compensate for the 10 per cent possible binary lenses.

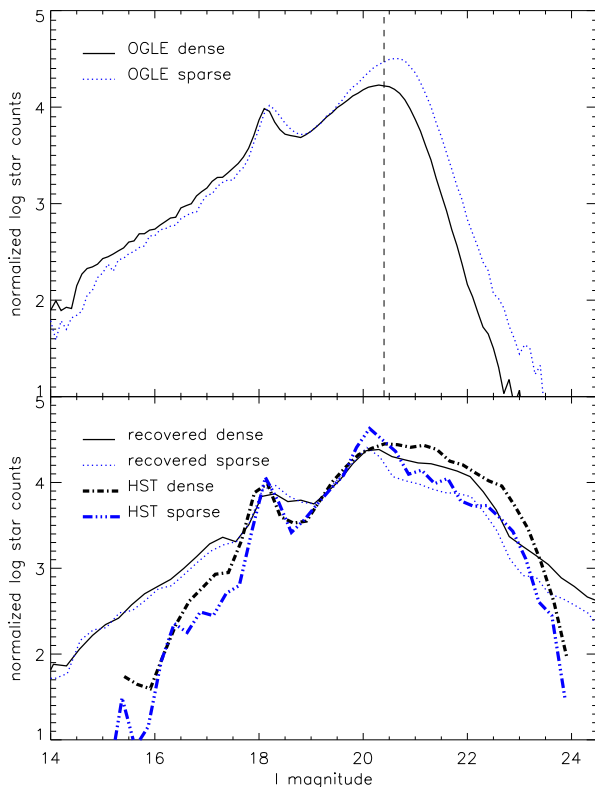


Figure 9. Upper panel: observed luminosity functions in two OGLE-II LMC fields, where the dotted and solid lines represent sparse (SC19) and dense (SC6) fields, respectively. The vertical line shows the cut-off at $I = 20.4$ mag. Lower panel: luminosity functions for the same fields recovered after applying the blending correction (see Section 6). Their shapes follow the prototype LFs of two HST fields (dense and sparse) used for the blending correction (thick dash-dotted lines).

We performed our simulations on both Bright and All Stars Samples with blending included. In addition, we repeated the analysis assuming no blending (*i.e.*, $f_s = 1$) in order to compare our results with other studies. We defined the Bright Stars Sample as stars with $N > 80$ and brighter than $I_{RC} + 1$ mag, where I_{RC} is the Red Clump stars’ centre on the colour-magnitude diagram. In the reference field LMC_SC1, this threshold was at 18.8 mag. The All Stars Sample comprised of all stars used in the search for microlensing events, *i.e.*, stars brighter than 20.4 mag and with at least 80 data points.

Fig. 8 shows the derived detection efficiencies for a wide range of time-scales for a typical dense field. Most sparse fields were observed for a shorter period of time (observations started about a year later than for dense fields). However, in our detection efficiency calculations we simulated microlensing events within the full time-span of the OGLE-II experiment, namely for t_0 within the range of $HJD = 2450446 - 2451874$. Therefore, the efficiency for fields observed for a shorter time is reduced by about 30 per cent, owing to the events which fall outside the simulated light curve. Only one field classified as sparse (LMC_SC12)

was monitored since the very beginning of the project and the microlensing detection efficiency for this field is comparable to the efficiencies for dense fields.

Fig. 8 also shows the detection efficiencies for the non-blended analysis of All and Bright Stars Samples (with $f_s = 1$ for all simulated events). The efficiency for Bright Stars with and without blending is higher than the corresponding efficiencies for All Stars Sample, as it is generally easier to recover events occurring on brighter stars.

The observed luminosity functions (LFs) of dense and sparse OGLE-II LMC fields are shown in the upper panel of Fig. 9. Blending is more severe in dense fields and it causes faint stars to ‘merge’ and form brighter objects, populating brighter parts of the luminosity functions. The bottom panel of Fig. 9 shows blending-free luminosity functions for a dense and sparse field, recovered using the blending distributions obtained by comparing OGLE and high-resolution HST images. The luminosity functions obtained from HST are shown as well. It is noticeable that the effect of over-populating the brighter parts and under-populating the faint end in blending-free LFs of dense fields has virtually disappeared after applying the correction. The recovered dense and sparse luminosity functions follow their prototypes from the HST everywhere except at the bright and very faint end. For stars brighter than $I \leq 17$ mag the HST images become saturated, which is reflected in the steeper luminosity functions at the bright end. The large scatter in the bright range is due to low number statistics in the HST’s small field-of-view (as compared to OGLE-II fields). The broadening of the Red Clump may also be caused by this effect, or could be due to the distance gradient along the OGLE field. The HST’s LFs of dense and sparse areas differ significantly, which is likely caused by the different mix of LMC bar and disk populations in these two fields.

In our Monte Carlo simulations, we drew an object from the original OGLE luminosity functions. Therefore we were not affected by the incompleteness of the bright end of the HST luminosity functions. Incompleteness in the faint end of the OGLE luminosity functions is partially recovered in the correction process, but also is negligible as the sensitivity for such faint stars is very low. Although our blending analysis successfully recovers the underlying stellar brightness distribution, it is still approximate as we used only two HST images to represent dense and sparse fields. In future, it would be interesting to expand this study with a detailed I -band high-resolution follow-up, using HST and/or other high-resolution instruments.

8 OPTICAL DEPTH ESTIMATE

We determined the optical depth using the All Stars Sample. For the two events found in the OGLE-II data we used the following standard equation for calculating the optical depth:

$$\tau = \frac{\pi}{2N_*T_{\text{obs}}} \sum_i^{N_{\text{ev}}} \frac{t_{Ei}}{\epsilon(t_{Ei})} \quad (6)$$

where $T_{\text{obs}} = 1428$ days is the time-span of all observations, $N_* = 11.8 \times 10^6$ is the total number of monitored stars (see Section 6), $N_{\text{ev}} = 2$ is the total number of events, t_{Ei}

Table 6. The optical depth for the two OGLE-II events.

event	t_E	$\epsilon(t_E)$	$\tau_i \times 10^{-7}$
efficiency not corrected for binary events			
OGLE-LMC-01	$57.2^{+4.7}_{-4.2}$	0.212174	0.25
OGLE-LMC-02	$23.8^{+6.0}_{-5.1}$	0.165536	0.13
total $\tau_{\text{LMC-O2}}$			0.38 ± 0.29
efficiency corrected for binary events			
OGLE-LMC-01	$57.2^{+4.7}_{-4.2}$	0.190957	0.28
OGLE-LMC-02	$23.8^{+6.0}_{-5.1}$	0.148982	0.15
total $\tau_{\text{LMC-O2}}$			0.43 ± 0.33

is the time-scale of each event detected with the efficiency of $\epsilon(t_{Ei})$. For the time-scales of these events we used the microlensing fit where blending was a free parameter (5-parameters model). The error in τ was calculated with the formula given by Han & Gould (1995a). For the original detection efficiency (i.e., not corrected for binary events), the optical depth was derived to be $\tau_{\text{LMC-O2}} = 0.38 \pm 0.29 \times 10^{-7}$. If the efficiency is corrected for non-detectability of binary lenses, the optical depth becomes $\tau_{\text{LMC-O2}} = 0.43 \pm 0.33 \times 10^{-7}$. Table 6 presents all calculations of the optical depth.

9 DISCUSSION

9.1 Optical depth

The OGLE-II LMC data analysed in this study covered about 4.5 sq. deg. of the sky over 4 years, which is clearly smaller than the data used by MACHO or EROS groups. However, it provides a completely independent data set to test the hypotheses concerning the presence of MACHOs in the Galactic halo.

Based on two the events we found the optical depth towards the LMC to be $\tau_{\text{LMC-O2}} = 0.43 \pm 0.33 \times 10^{-7}$. On one hand, this value is in $2\text{-}\sigma$ agreement with the $\tau_{\text{LMC}} = 1.0 \pm 0.3$ obtained by MACHO (Bennett 2005)⁵. If both OGLE-II events were caused by Machos, then they would contribute 8 ± 6 per cent to the total mass of the halo, according to model *S* from Alcock et al. (2000b).

On the other hand, our value of the optical depth is more consistent with a scenario of lensing due to the visible stellar LMC component alone (self-lensing), for which various estimates of the optical depth are present in the literature: $\tau_{\text{SL}} = (0.05 - 0.78) \times 10^{-7}$ (Gyuk et al. 2000), $\tau_{\text{SL}} = (0.24 - 0.36) \times 10^{-7}$ (Alcock et al. 2000b), $\tau_{\text{SL}} = 0.54 \times 10^{-7}$ (Belokurov et al. 2004).

⁵ Only 5 (#1, #8, #14, #15 and #18) out of 17 MACHO candidates occurred within OGLE-II fields. However, all of these events peaked before the first observations of OGLE-II. Therefore we can only confirm continuity of their constant baselines using our data.

Mancini et al. (2004) presented a detailed theoretical study of the halo and self-lensing optical depth and compared it with the results of MACHO. They simulated the disk and bar of the LMC and quantitatively derived a contribution from the LMC's own stars to the optical depth as $\tau < 6 \times 10^{-8}$. In the region of the LMC bar, where most OGLE-II fields are concentrated, they estimated the self-lensing optical depth to vary between 2 and 4×10^{-8} . The optical depth derived for two events we found in the OGLE-II data and averaged over all fields is in a perfect agreement with these estimates.

Also the time-scales of our two events seem to belong to the regime of self-lensing, especially the 57.2-days event, which lies exactly on the line for the self-lensing events in fig. 10 of Mancini et al. (2004). From the CMD of the LMC, it is apparent that both microlensed sources are coincident with an LMC population, indicating that they probably belong to the LMC. The locations of both events in the bar of the LMC also supports the self-lensing scenario.

If we assume that our two events are indeed due to self-lensing (i.e., we have zero events caused by the halo objects), we can derive an estimate for the upper limit of the Macho abundance in the halo of the Milky Way. We performed this analysis following the procedure similar to the one used by EROS in Tisserand et al. (2007), first estimating the number of expected events in the OGLE-II data set if the halo was entirely made of Machos, using model *S* (Alcock et al. 2000b). In this model the optical depth towards the LMC equals $\tau_{\text{total}}^S = 5.1 \times 10^{-7}$, which also includes a contribution from self-lensing and Galaxy disk lensing. Dark matter lensing solely had $\tau_{\text{Machos}}^S = 4.7 \times 10^{-7}$. For a so-called 'typical' mass of $0.4 M_{\odot}$, in OGLE-II we should expect 16 events. At the 95 per cent Poisson confidence level there are up to 3 events consistent with a zero detection. This divided by a number of expected events gives the upper limit on the mass fraction of about 19 per cent. This translates to an upper limit on the optical depth due to Machos of $\tau_{0.4M_{\odot}} < 0.9 \times 10^{-7}$. If blending is neglected in the All Stars Sample the numbers are somewhat larger: about 9 expected events would put a limit of $\tau_{0.4M_{\odot}} < 1.6 \times 10^{-7}$.

Fig. 10 shows the dependence of the number of expected events on the mass of the lensing objects for the blended and non-blended approach. Fig. 11 shows the 95 and 90 per cent confidence limits on the halo Macho mass fraction for a wide range of masses. It also compares our results with the results from EROS and MACHO. This figure clearly shows that the OGLE-II project is the most sensitive to events caused by Machos with masses between 0.01 and $0.2 M_{\odot}$. For this range of masses, we can place an even tighter upper-limit of about 10 per cent (at 95 per cent confidence) on the abundance of compact dark matter objects in the Galactic halo. A more detailed theoretical analysis will be presented in a forthcoming paper (Calchi Novati, Mancini, Scarpetta et al., in preparation).

For the sake of comparison with the results of the EROS group, we also performed the above analysis narrowing the stars sample only to the bright stars. In each field, our Bright Sample consisted of about 20 - 30 per cent of stars present in All Stars Sample, with a total over all fields of about 1.9 million. After correction for blending, the number of monitored stars was about 3.6 million. In the Bright Sample of OGLE-II, we have not found any events. Ac-

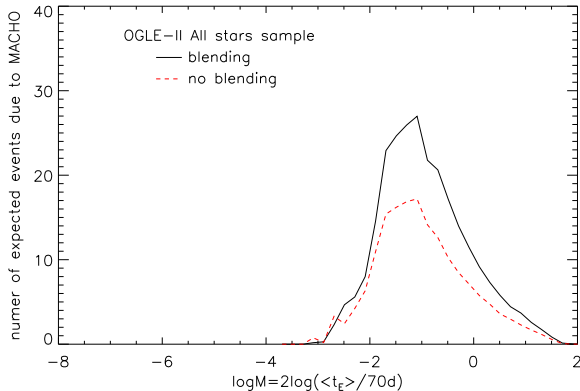


Figure 10. The number of microlensing events caused by Machos expected to be seen in the OGLE-II data, for blended and non-blended approaches.

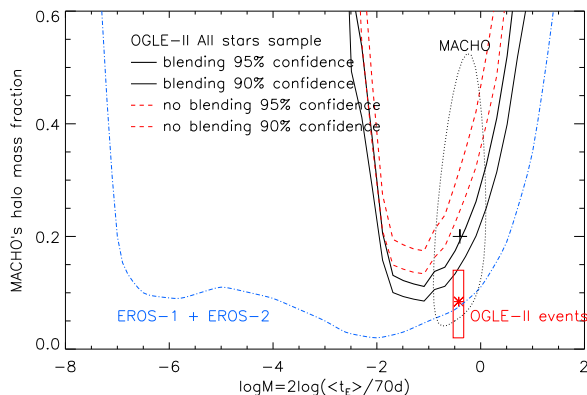


Figure 11. Mass fraction in compact dark halo objects as a function of the mass of the lensing objects. The red box with a star shows the value for the two OGLE-II events assuming they are caused by halo lenses. Solid and dashed lines show OGLE-II upper limits assuming both OGLE events are due to self-lensing. Also shown are the results of the MACHO collaboration (dotted line) and the upper limit derived by the EROS group (dot-dashed line).

According to the full S model of Alcock et al. (2000b), we should expect about 9 events to be caused by lenses of mass $0.4M_{\odot}$, including events due to self-lensing. If we neglect blending, then we expect 6 events. The total optical depth towards the LMC is therefore estimated to be $\tau_{0.4M_{\odot}} < 1.6 \times 10^{-7}$ ($\tau_{0.4M_{\odot}} < 2.6 \times 10^{-7}$) with (without) the full blending correction. The calculated upper-limit is very high due to the fact that OGLE-II has much smaller sky coverage and shorter time-baseline compared to the combined EROS-I and EROS-II projects. However, a combined study of OGLE-II and OGLE-III data will be conducted in the near future and should be able to yield constraints of even stronger magnitude than those given by the EROS collaboration (Wyrzykowski et al. 2008, Wyrzykowski et al., in preparation).

9.2 Blending

As has been discussed above, we did not have HST data for all OGLE-II fields. Therefore we chose to use the two selected HST fields and consider these as being representative of two different density levels. In this way we recover only an approximation to the underlying real luminosity function for each field.

In order to check how our selection of HST stars affects the result, we repeated the whole analysis for a different cut on the HST stars magnitude, namely 2.5 mag (instead of 3.5 mag) below the brightness of the OGLE objects. This translates to a minimal allowed blending fraction of 10 per cent. We then rederived the blending distributions and the distributions for the number of HST stars in a single OGLE object. These distributions were obviously different compared to the original 3.5 mag cut; for both sparse and dense fields, there was nearly no blending in the brightest magnitude bin. For the fainter stars, the distributions indicated a level of blending similar to that which was found previously, but with slightly less pronounced features for small f_S .

In a similar manner to that described in Section 6, we estimated the total number of monitored stars and found about 9.2×10^6 stars. Then we also repeated the efficiency calculation including these new blending distributions. It was similar to the original efficiency to within 2 per cent. The detection efficiencies (corrected for binary events) for the two events were found to be $\epsilon(t_E = 57.2) = 0.214$ and $\epsilon(t_E = 23.8) = 0.165$. Since these efficiencies are similar to previous values while the number of monitored stars is reduced, we find that this yields a somewhat larger optical depth of $\tau_{\text{HST}2.5} = (0.49 \pm 0.37) \times 10^{-7}$. This is, however, still consistent with our original value, indicating little sensitivity of the optical depth on the depth of blending stars' magnitude limit.

As an extreme case we also considered neglecting blending completely in our All Stars Sample. In this case, we find that there are only about 5.5 million sources with $f_S = 1$. The detection efficiency was obtained as described above and is shown on Fig. 8. It was larger than in the case when blending is taken into account by about 20 per cent. However, this does not cancel out entirely with the reduction in the number of monitored sources. Using these numbers with non-blended model time-scales (Table 5) leads to a larger value for the optical depth of $\tau = (0.72 \pm 0.55) \times 10^{-7}$, where we have used the detection efficiencies corrected for lack of binary events.

This indicates that neglecting blending favours larger values of the optical depth, emphasising the importance of carrying out a careful analysis of blending when dealing with All Stars samples in order to obtain reliable optical depth results towards the LMC.

10 CONCLUSIONS

In the search for microlensing events in OGLE-II data towards the Large Magellanic Cloud, we found two events. The total optical depth for all 21 OGLE-II LMC fields, covering about 4.5 square degrees, was derived for the All Stars Sample (with a limit of $\langle I \rangle \leq 20.4$ mag) as $\tau_{\text{LMC-O2}} =$

$0.43 \pm 0.33 \cdot 10^{-7}$. If both events were caused by Machos, this would imply that their comprise 8 ± 6 per cent of the halo by mass.

However, the value of the optical depth and the characteristics of the events are consistent with the self-lensing scenario, in which lensing towards the LMC occurs only between sources and lenses both located in the Cloud. From this, we can constrain the presence of compact dark matter objects in the Milky Way's halo and we find that our results are compatible with no detection. The upper limit is found to be 19 per cent for $M_{Macho} = 0.4M_{\odot}$ and 10 per cent for masses between 0.01 and $0.2 M_{\odot}$. It is worth emphasising that in our study we probed mainly the bar of the LMC, similarly to the MACHO project. However, our results and conclusions are closer to the ones of the EROS collaboration, which probed different regions of the LMC.

The sensitivity of the OGLE-II experiment is limited to a relatively short time span and sky coverage. However, the results presented in this paper will be soon strengthened and supplemented with the analysis of the 8-year OGLE-III data.

Future photometric and astrometric surveys may confirm the lensing origin of most of events detected so far and the new ones by high-resolution imaging or precise astrometry, allowing for measuring the distances to the sources and lenses or their velocities.

ACKNOWLEDGEMENTS

The authors would like pay tribute to the late Bohdan Paczyński, as the subject of this work was always a subject of interest for him. We are grateful to the referee, Andy Gould for his comments and assistance in combining MACHO and OGLE data sets for measure the colour of OGLE-LMC-01. We also would like to thank for their help at various stages of this work to Drs Wyn Evans, Subo Dong, Luigi Mancini, Sebastiano Calchi-Novati, Gaetano Scarpetta, Hongsheng Zhao and Daniel Faria. LW, SK, MCS and JS acknowledge generous support from the European Community's FR6 Marie Curie Programme, Contract No. MRTN-CT-2004-505183 "ANGLES". MCS also acknowledges support from the STFC-funded "Galaxy Formation and Evolution" program at the Institute of Astronomy, University of Cambridge. The OGLE project is partially supported by the Polish MNiSW grant N20303032/4275. JS also acknowledges support through the Polish MNiSW grant no. N20300832/070.

REFERENCES

Afonso C., Albert J. N., Alard C., Andersen J., Ansari R., et al. 2003, *Astronomy & Astrophysics*, 404, 145
 Alard C., Lupton R. H., 1998, *Astrophysical Journal*, 503, 325
 Alcock C., Akerloff C. W., Allsman R. A., Axelrod T. S., et al. 1993, *Nature*, 365, 621
 Alcock C., Allsman R. A., Alves D. R., Axelrod T. S., et al. 2000a, *Astrophysical Journal*, 541, 734
 Alcock C., Allsman R. A., Alves D. R., Axelrod T. S., et al. 2000b, *Astrophysical Journal*, 542, 281

Alcock C., Allsman R. A., Alves D. R., et al. 2001, *Astrophysical Journal Supplement Series*, 136, 439
 Aubourg E., Bareyre P., Brehin S., Gros M., et al. 1993, *Nature*, 365, 623
 Belokurov V., An J., Evans N. W., Hewett P., et al. 2005, *MNRAS*, 357, 17
 Belokurov V., Evans N. W., Du Y. L., 2003, *MNRAS*, 341, 1373
 Belokurov V., Evans N. W., Le Du Y., 2004, *MNRAS*, 352, 233
 Bennett D. P., 2005, *Astrophysical Journal*, 633, 906
 Bennett D. P., Becker A. C., Tomaney A., 2005, *Astrophysical Journal*, 631, 301
 Bond I. A., Rattenbury N. J., Skuljan J., et al. 2002, *MNRAS*, 333, 71
 Calchi Novati S., Paulin-Henriksson S., An J., et al. 2005, *Astronomy & Astrophysics*, 443, 911
 de Jong J. T. A., Widrow L. M., Cseresnyes P., Kuijken K., Crofts A. P. S., Bergier A., Baltz E. A., Gyuk G., Sackett P. D., Uglesich R. R., Sutherland W. J., 2006, *Astronomy & Astrophysics*, 446, 855
 Feeney S. M., Belokurov V., Evans N. W., An J., Hewett P. C., Bode M., Darnley M., Kerins E., Baillon P., Carr B. J., Paulin-Henriksson S., Gould A., 2005, *Astrophysical Journal*, 130, 84
 Gould A., 2004, *Astrophysical Journal*, 606, 319
 Gyuk G., Dalal N., Griest K., 2000, *Astrophysical Journal*, 535, 90
 Hamadache C., Le Guillou L., Tisserand P., Afonso C., et al. 2006, *Astronomy & Astrophysics*, 454, 185
 Han C., Gould A., 1995a, *Astrophysical Journal*, 449, 521
 Han C., Gould A., 1995b, *Astrophysical Journal*, 447, 53
 Holtzman J. A., Afonso C., Dolphin A., 2006, *Astrophysical Journal Supplement Series*, 166, 534
 Kallivayalil N., Nguyen H. T., Werner M. W., Alcock C., Patten B. M., Stern D., 2004, in *Bulletin of the American Astronomical Society Vol. 36 of Bulletin of the American Astronomical Society*, Spitzer Space Telescope Observations of the Aftermath of Microlensing Event MACHO-LMC-5. pp 725
 Kallivayalil N., Patten B. M., Marengo M., Alcock C., Werner M. W., Fazio G. G., 2006, *Astrophysical Journal Letters*, 652, L97
 Keller S. C., Bessell M. S., Cook K. H., Geha M., Syphers D., 2002, *Astrophysical Journal*, 124, 2039
 Kozłowski S., 2007, PhD Thesis, Manchester University
 Kozłowski S., Woźniak P. R., Mao S., Wood A., 2007, *Astrophysical Journal*, 671, 420
 Mancini L., Calchi Novati S., Jetzer P., Scarpetta G., 2004, *Astronomy & Astrophysics*, 427, 61
 Paczyński B., 1986, *Astrophysical Journal*, 304, 1
 Paczyński B., 1996, *ARA&A*, 34, 419
 Park B.-G., DePoy D. L., Gaudi B. S., Gould A., et al. 2004, *Astrophysical Journal*, 609, 166
 Popowski P., Griest K., Thomas C. L., Cook K. H., Bennett D. P., et al. 2005, *Astrophysical Journal*, 631, 879
 Smith M. C., Woźniak P., Mao S., Sumi T., 2007, *MNRAS*, 380, 805
 Sumi T., Abe F., Bond I. A., Dodd R. J., et al. 2003, *Astrophysical Journal*, 591, 204
 Sumi T., Woźniak P. R., Udalski A., Szymański M., Kubiak M., Pietrzyński G., Soszyński I., Żebruń K., Szcwarczyk O.,

- Wyrzykowski L., Paczyński B., 2006, *Astrophysical Journal*, 636, 240
- Szymański M. K., 2005, *Acta Astronomica*, 55, 43
- Tisserand P., Le Guillou L., Afonso C., Albert J. N., The EROS-2 Collaboration et al. 2007, *Astronomy & Astrophysics*, 469, 387
- Udalski A., 2003, *Acta Astronomica*, 53, 291
- Udalski A., Kubiak M., Szymański M., 1997, *Acta Astronomica*, 47, 319
- Udalski A., Szymański M., Kałużny J., Kubiak M., Krzemiński W., Mateo M., Preston G. W., Paczyński B., 1993, *Acta Astronomica*, 43, 289
- Udalski A., Szymański M., Kałużny J., Kubiak M., Mateo M., Krzemiński W., Paczyński B., 1994, *Acta Astronomica*, 44, 227
- Woźniak P., Paczyński B., 1997, *Astrophysical Journal*, 487, 55
- Woźniak P. R., 2000, *Acta Astronomica*, 50, 421
- Wyrzykowski L., Kozłowski S., Belokurov V., Smith M. C., Skowron J., Udalski A., 2008, in *Proceedings of the Manchester Microlensing Conference: The 12th International Conference and ANGLES Microlensing Workshop*, eds. E. Kerins, S. Mao, N. Rattenbury and L. Wyrzykowski PoS(GMC8)011, The OGLE search for microlensing events towards the LMC
- Wyrzykowski L., Udalski A., Mao S., Kubiak M., Szymański M. K., Pietrzyński G., Soszyński I., Szewczyk O., 2006, *Acta Astronomica*, 56, 145
- Yock P. C. M., 1998, in Sato H., Sugiyama N., eds, *Frontiers Science Series 23: Black Holes and High Energy Astrophysics "MOA" - The JAPAN-NZ Gravitational Microlensing Project*. pp 375